

# The Anfeq post-collisional Pan-African high-K calc-alkaline batholith (Central Hoggar, Algeria), result of the LATEA microcontinent metacratonization

Kaissa Acef<sup>a</sup>, Jean Paul Liégeois<sup>b,\*</sup>, Aziouz Ouabadi<sup>a</sup>, Louis Latouche<sup>c,✱</sup>

<sup>a</sup> Institut des Sciences de la Terre, Université des Sciences et de la Technologie Houari Boumediene, B.P. 2, Dar el Beida, Alger, Algeria

<sup>b</sup> Isotopic Geology, African Museum, B-3080 Tervuren, Belgium

<sup>c</sup> CNRS FRE2456, Minéralogie, Muséum National d'Histoire Naturelle, 61 rue Buffon, F75005 Paris, France

Received 13 November 2002; accepted 12 June 2003

## Abstract

The Anfeq batholith (or composite laccolith) occupies a large surface (2000 km<sup>2</sup>) at the northern tip of the Laouni terrane, just south of Tamanrasset in Hoggar. It is granodioritic to granitic in composition and comprises abundant enclaves that are either mafic microgranular enclaves (MME) or gneissic xenoliths. It intruded an Eburnian ( $\approx 2$  Ga) high-grade basement belonging to the LATEA metacraton at approximately 608 Ma (recalculated from the U–Pb dating of [Tectonics 5 (1986) 955]) and cooled at approximately 4 kbar, with a temperature of about 750 °C. This emplacement occurred mainly along subhorizontal thrust planes related to Pan-African subvertical mega-shear zones close to the attachment zone of a strike-slip partitioned transpression system. Although affected by some LILE mobility, the Anfeq batholith can be ascribed to a high-K calc-alkaline suite but characterized by low heavy REE contents and high LREE/HREE ratios. The MME belong to the Anfeq magmatic trend while some xenoliths belong to Neoproterozoic island arc rocks.

The Anfeq batholith defines a Nd–Sr isotopic initial ratios trend ( $\epsilon_{\text{Nd}}/({}^{87}\text{Sr}/{}^{86}\text{Sr})_i$  from  $-2.8/0.7068$  to  $-11.8/0.7111$ ) pointing to a mixing between a depleted mantle and an old Rb-depleted granulitic lower crust. Both sources have been identified within LATEA and elsewhere in the Tuareg shield ( $\epsilon_{\text{Nd}}/({}^{87}\text{Sr}/{}^{86}\text{Sr})_i$  of  $+6.2/0.7028$  for the depleted mantle,  $-22/0.708$  for the old lower crust).

The model proposed relates the above geochemical features to a lithospheric delamination along the subvertical mega-shear zones that dissected the rigid LATEA former passive margin without major crustal thickening (metacratonization) during the general northward tectonic escape of the Tuareg terranes, a consequence of the collision with the West African craton. This delamination allowed the uprise of the asthenosphere. In turn, this induced the melting of the asthenosphere by adiabatic pressure release and of the old felsic and mafic lower crust due to the high heat flow. A gradient in the mantle/crust ratio within the source of the Pan-African magmatism is observed in LATEA from the northeast (Egéré-Aleksod terrane) where rare plutons are rooted within the Archaean/Eburnian basement to the southwest (Laouni terrane) where abundant batholiths, including Anfeq, have a mixed signature. Some mantle melts with only slight crustal contamination (Laouni troctolitic layered intrusions) are even present. This suggests that the southern boundary of LATEA microcontinent is not far south of the Tuareg shield.

© 2003 Elsevier Ltd. All rights reserved.

**Keywords:** High-K calc-alkaline series; Post-collisional; Pan-African; Hoggar; Metacraton

## 1. Introduction

The studies of ancient orogenic magmatism have often focused on active margins, or in areas considered as

former active margins. The spectacular volcanic and plutonic activity of the Andean cordillera has been classically opposed to the current tranquillity of the West African coast. Now, it is however clear that the post-collisional magmatism is of paramount importance (e.g. Liégeois, 1998). The Tuareg shield (Black et al., 1994; Fig. 1) is composed on 40% of its surface by granitoids, most of them being post-collisional and high-K calc-alkaline in nature, with some late alkaline to per-alkaline manifestations. However, their precise tectonic

\* Corresponding author. Tel./fax: +32-2-650-2252.

E-mail addresses: kacef@ yahoo.fr (K. Acef), jean-paul.liegeois@africanmuseum.be (J.P. Liégeois), ouabadi@yahoo.fr (A. Ouabadi).

✱ Deceased, June 2003.

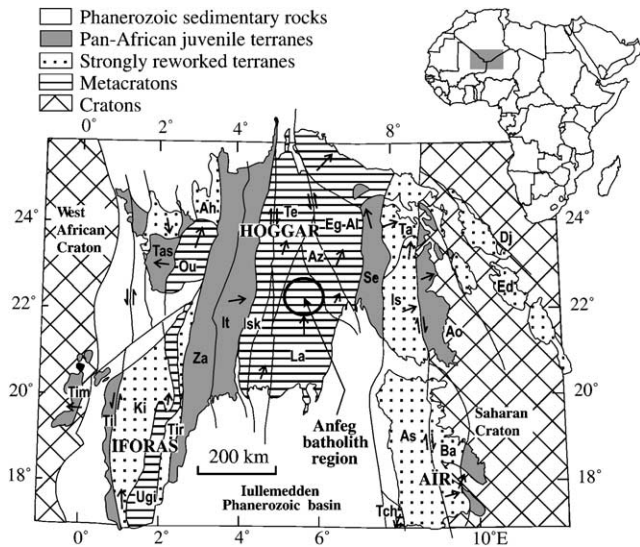


Fig. 1. Tuareg shield terrane map (from Black et al., 1994). Solid arrow = movement direction. From east to west, the 23 terranes are Djanet (Dj), Edembo (Ed), Aouzegueur (Ao), Barghot (Ba), Assodé-Issalane (As-Is), Tchilit (Tch), Tazat (Ta), Serouenout (Se), Egéré-Aleksod (Eg-Al), Azrou-n-Fad (Az), Tefedest (Te), Laouni (La), Iskel (Isk), In Teidini (It), Tin Zaouatene (Za), Tirek (Tir), Ahnet (Ah), In Ouzzal (Ou), Iforas granulitic unit (Ugi), Tassendjanet (Tas), Kidal (Ki), Tilemsi (Til), Timétrine (Tim).

setting and geochemistry may vary (Liégeois et al., 1998). The Anfeq batholith is a particular case, not usually taken into account. Indeed, we will show here that the Anfeq batholith intruded into a former passive margin during its post-collisional dismembering without any major crustal thickening during the collision itself. As a modern analogue, the India former passive margin has been poorly affected by the Himalayan collision, having been mainly overthrust by Asian nappes. This dismembering was mainly marked by horizontal displacements along mega-shear zones accompanied by mid-crustal thrusts and by retrogressive greenschist to lower amphibolite facies metamorphisms (Liégeois et al., 2003, this issue and references therein). This corresponds to the notion of metacraton (Abdelsalam et al., 2002), i.e. a craton that has been remobilized during an orogenic event but is still recognisable.

## 2. The Tuareg shield terranes

The Tuareg shield belongs to the Trans-Saharan Pan-African belt. With an E–W width of more than 1300 km, it is located between the West African craton to the west and the Saharan metacraton to the east (Black et al., 1994; Liégeois et al., 1994). It is composed of 23 recognized terranes (Fig. 1) comprising Archaean, Palaeoproterozoic and Neoproterozoic material that were assembled during the Pan-African orogeny (mainly 750–525 Ma).

The Tuareg terranes were assembled during two main phases (Liégeois et al., 1994). A first intense collision occurred between the Saharan craton (former passive margin) and the easternmost Tuareg terranes at around approximately 700 Ma. A second more oblique collision occurred to the west with the West African craton; it began at approximately 630 Ma and its latest post-collisional movements and magmatism spread till approximately 525 Ma. This 100 Ma long period is mainly characterized by subvertical mega-shear zones, intrusion of high-K calc-alkaline plutons locally followed by alkaline–peralkaline magmatism, and high temperature upper greenschist or lower amphibolite facies metamorphism.

Diachronisms occurred between terranes but similar successions have been deciphered in several terranes, e.g. in Air and Adrar des Iforas (Ba et al., 1985; Caby and Andreopoulos-Renaud, 1987; Caby et al., 1989; Liégeois et al., 1987, 1994, 1996, 1998): (1) pre-collisional TTG series linked to magmatic arcs in the terranes of Aouzegueur ( $\approx 730$  Ma), Tilemsi (730–720 Ma) and Kidal (650–630 Ma); (2) early post-collisional migmatitic potassic leucogranites linked to collapse in the terrane of Assodé ( $\approx 666$  Ma); (3) major post-collisional high-K calc-alkaline batholiths (630–580 Ma), linked to transpressive movements along major shear zones in most Tuareg terranes; (4) late post-collisional alkaline–peralkaline high-level plutonism and volcanism linked to slight transtensional movements along mega-shear zones as early as approximately 592 Ma in western Hoggar (Hadj-Kaddour et al., 1998) and ending at approximately 525 Ma in Central Hoggar (Paquette et al., 1998).

The above studies concern terranes deeply affected by the Pan-African orogeny. In the Tuareg shield however, some terranes are known to have escaped most of the Pan-African events, such as the In Ouzzal terrane (e.g. Caby, 1996) where very-high temperature metamorphic assemblages are preserved ( $>1000$  °C, 10–11 kbar; Kienast et al., 1996; Ouzegane and Boumaza, 1996). The Pan-African orogeny has only marked the In Ouzzal terrane through greenschist retrogression along narrow shear zones and through some high-level generally circular plutons displaying sharp contacts with the country-rocks.

An intermediate case is the LATEA composite terrane in Central Hoggar, which is formed by the Laouni, Azrou N’Fad, Tefedest, and Egéré-Aleksod (hence the acronym “LATEA”, Fig. 2; Liégeois et al., 2003). These terranes are composed of Archaean and Eburnian basement (Latouche and Vidal, 1974; Bertrand et al., 1986; Peucat et al., 2003) with frequent unaltered granulitic and amphibolitic Eburnean parageneses (Belhai and Ouzegane, 2000; Ouzegane et al., 2001).

This area, roughly corresponding to Central Hoggar, has been initially described as a “Suggarian” basement

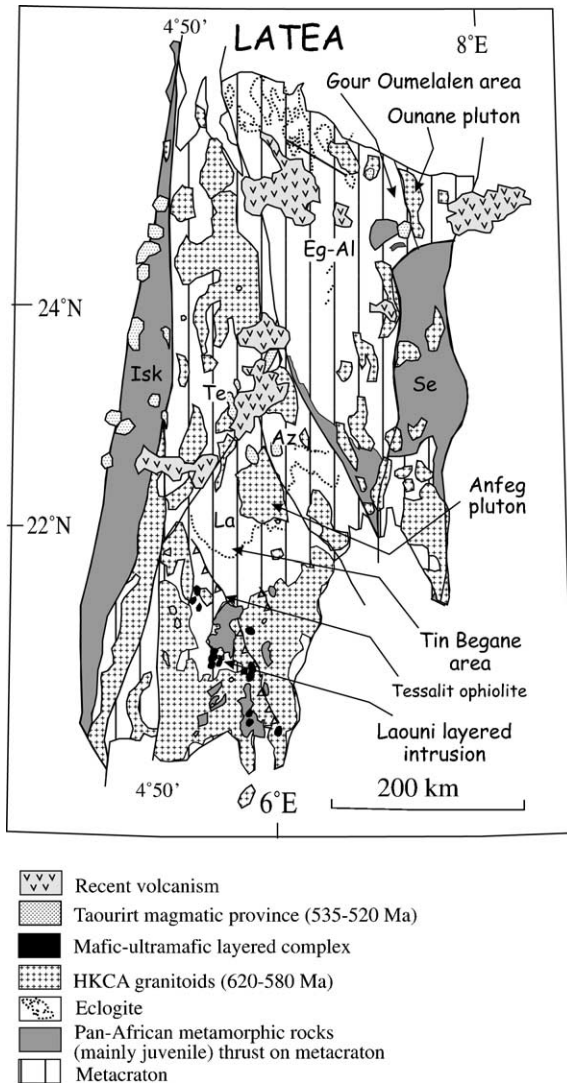


Fig. 2. Present situation of LATEA showing the preserved Archaean–Palaeoproterozoic basement (metacraton) dissected in four terranes (La = Laouni, Az = Azrou-n-Fad, Te = Tefedest, Eg-Al = Egéré-Aleksod), the thrust juvenile material (at approximately 850 Ma [Isk = Iskel], approximately 685 Ma and even probably later [Se = Serouenout]), the high-K calc-alkaline (HKCA) batholiths (620–580 Ma), the mantle-derived mafic–ultramafic layered complexes, the alkaline-alkali-calcic plutons (Taourirts) and the recent Tuareg volcanism mainly located in LATEA metacraton (from Liégeois et al., 2003, this issue). Main areas discussed in the text are localized.

(i.e. amphibolite-granulitic basement and associated granitoids) in which occurred “Pharusian” basins (i.e. greenschist facies assemblages and crosscutting igneous rocks). Later studies, integrating structural and geochronological data (e.g. Bertrand et al., 1986; Liégeois et al., 2003, this issue and references therein) demonstrated that this regional structure is an Archaean to Palaeoproterozoic basement partly reworked during the Pan-African ( $\approx 0.6$  Ga). This reworking is marked by: (1) overthrusts of Neoproterozoic volcano-sedimentary rocks bearing an oceanic character; (2) major shear

zones associated with greenschist to low amphibolite retrograde metamorphism; (3) intrusion of various granitoids. The overthrusting of oceanic material, including eclogites and ophiolites, occurred at approximately 685 Ma to the south of Anfeq in the Tin Begane area and induced local retromorphic greenschist metamorphism and mylonitic shears into the basement (Bertrand et al., 1986; Liégeois et al., 2003, this issue). This can be considered as the effects of oceanic arc accretions onto a former passive margin. After these oceanic accretions, LATEA was dissected, during a post-collisional phase into several terranes through movements of several hundred of km along mega-shear zones. The movements along these mega-shear zones were accompanied by the intrusion of granitoids along these mega-shear zones and along associated subhorizontal thrust planes, among which the Anfeq batholith. These tectonic and magmatic events led to a partial reworking of the LATEA microcontinent (metacratonization; Liégeois et al., 2003).

### 3. The Anfeq batholith

The Anfeq batholith is located within the Laouni terrane to the southeast of Tamanrasset (Figs. 2 and 3). It intruded at  $608 \pm 7$  Ma (U–Pb zircon; Bertrand et al., 1986, recalculated following Ludwig, 1999). This is a large flat elliptical NNW–SSE oriented granitic surface ( $\sim 2000$  km<sup>2</sup>), broadly bounded by mega-shear zones. To the NW, occur the NE oriented East-Tamanrasset shear zone and to the NE, the NNW oriented East Anfeq sinistral shear zone, which constitutes the eastern limit of the Laouni terrane (Fig. 3). The Anfeq batholith is cut later by several large NNE–SSW-oriented mylonitic faults. One of these faults extends from Amarhalrhal to Oued Teddesine and separates the Anfeq batholith into two lobes of similar surface (Fig. 3). Satellite bodies are located to the south and to the west of the main body such as the Tifferkit, Amsel and Tin Amzi intrusions. Crosscutting circular plutons such as In Tounine or Debnat (Fig. 3) belong to a younger family bearing topaz and W–Sn mineralizations (535–525 Ma, Ar–Ar method; Cheilletz et al., 1992).

The Anfeq batholith crosscuts Eburnian high-grade metamorphic rocks ( $\approx 2$  Ga; Bertrand et al., 1986; Ouzegane et al., 2001) composed of migmatitic gneisses, platten-quartz-bearing banded gneiss, biotite-garnet-sillimanite gneiss, olivine-spinel marble, amphibolite and garnet pyroxenite. Well-preserved granulitic relics are common, particularly in garnet pyroxenite: this granulitic metamorphism displays a clockwise P–T–t path from 800 °C and 10 kbar through 700 °C and 6 kbar, with always low water activity ( $a_{H_2O} = 0.1–0.5$ ). This path is related to an Eburnian crustal thickening during collisional tectonics (Ouzegane et al., 2001).

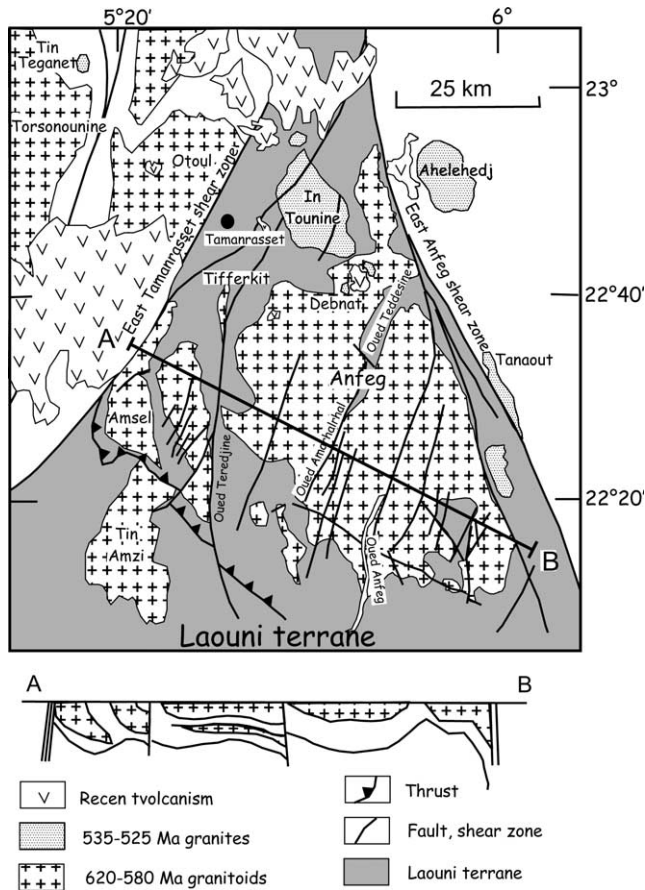


Fig. 3. The Anfeq batholith and surrounding geological map (adapted from Guérangé and Byramjee, 1957; Bertrand et al., 1986; Cheilletz et al., 1992) and the interpretative highly schematic cross section from the authors.

The Anfeq batholith is made of a series of granitic sheets (Fig. 3, cross section) intruded along subhorizontal thrust planes having acted under upper amphibolite facies conditions. In detail, two schistositities can be observed (Fig. 4; Bertrand et al., 1986): (1) a first schistosity (Sp1) is gently dipping to the NE and is

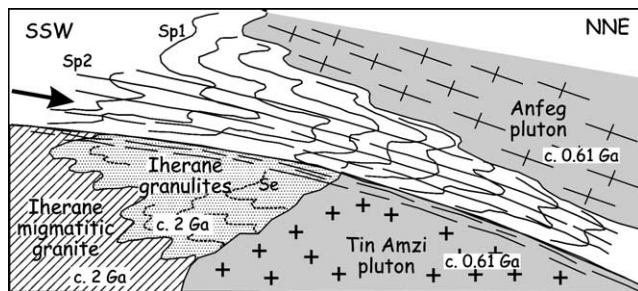


Fig. 4. Anfeq—Tin Amzi cross section from Bertrand et al. (1986). Se is the Eburnian schistosity in the granulites; Sp1 and Sp2 are the Pan-African schistositities, respectively in lower amphibolite and in upper greenschist metamorphic facies. The Iherane granulites and granite have been dated at approximately 2 Ga and Anfeq and Tin Amzi granites at approximately 0.61 Ga (recalculated from Bertrand et al., 1986).

associated with a conspicuous NE stretching lineation strongly reworking the Eburnian gneisses; (2) a second schistosity (Sp2) at low angle (<30°) with Sp1 developed with tight overturned folds with NW-trending axes. The associated metamorphism is epidote amphibolite facies. Sp2 can grade to strong flat shear zones indicating a NNE sense of movements for the upper unit. These two phases are interpreted within a single progressive tangential deformation during waning metamorphism (Bertrand et al., 1986). The Anfeq batholith intruded syn-kinematically during the Sp2 deformation, i.e. during the second part of the Pan-African deformation that affected variably the granitoids with the local development of tangential shear zones. The Tin Amzi granite (Fig. 4) corresponds to a slightly earlier pulse of the Anfeq batholith. The Anfeq batholith is actually composed of a succession of thin granitic layers alternatively isotropic and mylonitic. The abundance of subhorizontal metasedimentary xenoliths enhances this structure that has been described as “migmatitic” by Guérangé and Byramjee (1957).

Close to subvertical shear zones, the foliation affecting the Anfeq batholith becomes also subvertical and subsolidus fabrics predominate. This can be ascribed to a long-lasting tectonic activity along these mega-shear zones. Metamorphic conditions waned slowly as titanite from Tin Amzi pluton gave a cooling age of  $578 \pm 6$  Ma (Bertrand et al., 1986).

The very end of the Laouni terrane deformations consists of brittle faults well depicted on aerial photographs. Their main direction is NNE–SSW to NE–SW, likely to be in relation with the main shear zone bordering the Laouni terrane to the east while secondary directions (WNW–ESE, NW–SE, NNW–SSE, N–S) are also observed (Moulahoum, 1988). The brittle deformation can be correlated with the emplacement of the late high-level (abundant miaroles) circular topaz-bearing plutons dated at 535–525 Ma (Cheilletz et al., 1992). This age interval encompasses the youngest high-level ring complex emplaced at  $523 \pm 1$  Ma (Tioueine massif; Paquette et al., 1998) in the “Taourirt” province (Azzouni-Sekkal and Boissonnas, 1993; Azzouni-Sekkal et al., 2003; Fig. 2) and the age of the regional greenschist facies metamorphism dated by the Sm–Nd method in the Tin Begane area, south of Anfeq ( $522 \pm 27$  Ma; Liégeois et al., 2003).

Numerous dykes cut the Anfeq batholith. Most are NNE-oriented quartz dykes; aplitic and pegmatitic dykes are more variably oriented and contain tourmaline and amphibole. Some thin dykes bear green micas and look like greisen although none of the dykes bear economic mineralization (Guérangé and Byramjee, 1957). Some of them are probably linked to the late topaz-bearing high-level plutons.

Also, a few small post-collisional ultramafic–mafic layered intrusions have been described south of Anfeq

(Cottin et al., 1998): these layered intrusions comprise troctolitic and noritic cumulate series. They are emplaced into Anfeq-type syn-kinematic granitoids and older metamorphic rocks and are free from metamorphic recrystallization. In the Anfeq batholith, we have mapped one large, several hundred metres thick dyke of an orthopyroxene-bearing quartz monzodiorite (quartz jotunite). It is not known if this dyke is linked to the Laouni noritic layered intrusion event.

#### 4. Petrography and mineralogy

The Anfeq batholith is composed of two main types of granitoids, numerous enclaves and a series of cross-cutting dykes. Mineral analyses used hereafter are not listed in a table but are available from the authors.

##### 4.1. Biotite granodiorite/monzogranite

This granitoid is characterized by K-feldspar megacrysts (up to 7 cm) giving the rock a pink and porphyroid appearance. These megacrysts ( $0.56 < X_{\text{orth}} < 0.97$ ) determine a marked planar foliation. Quartz is present as large crystals with undulose extinction and as xenomorphic recrystallized crystals, as a response to the deformation. Plagioclase forms automorphic tabular crystals. This is an oligoclase with quite homogeneous compositions ( $0.21 < X_{\text{an}} < 0.25$ ). It is sometimes kinked or even broken. In the latter case, biotite and titanite frequently crystallized perpendicular to the fracture. Biotite ( $0.47 < X_{\text{Mg}} < 0.57$ ;  $0.358 < \text{Ti} < 0.478$ ) forms small dark brown crystals dispersed in the rock. Aggregates of several biotite crystals are often stretched and flakes have shredded borders. Its abundance is variable, giving to this granite a mesocratic to leucocratic aspect.

##### 4.2. Amphibole-biotite granodiorite/monzogranite

This granitoid presents the same characteristics as the biotite granite, having in addition an amphibole (Mg-hornblende to Fe-edenite:  $1.397 < \text{Al}_t < 1.682$ ). Plagioclase is zoned, showing therefore a wider compositional variation ( $0.06 < X_{\text{an}} < 0.42$ ). Biotite composition is also more variable ( $0.39 < X_{\text{Mg}} < 0.55$ ) than in the biotite granitoid. Quartz is partially recrystallized and displays undulose extinction while plagioclase and biotite crystals are often kinked.

##### 4.3. Enclaves

Most of the Anfeq enclaves are microgranular and mafic but xenoliths are also abundant particularly near contacts. The microgranular mafic enclaves (MME) comprise mainly plagioclase, biotite and hornblende and

have a doleritic texture. Quartz and K-feldspar are subordinate. Plagioclase presents euhedral stubby laths. Biotite ( $0.39 < X_{\text{Mg}} < 0.43$ ) is elongated, highly pleochroic, with numerous oxide inclusions. Amphibole has a composition ranging from Fe-edenite to Fe-hornblende. Titanite, epidote, apatite and zircon are the accessories. These MME show mingling–mixing textures such as quartz ocellas and large plagioclase crystals with reverse and patchy zoning.

Xenoliths, generally made of metasedimentary country-rocks, include fine-grained granoblastic amphibolite displaying a migmatitic structure, unknown within nearby country-rocks (sample An<sub>11</sub>).

##### 4.4. Dykes

Crosscutting aplitic or pegmatitic dykes are not studied here except the large one containing orthopyroxene (sample An<sub>7</sub>). The latter is an enstatite often located inside amphibole. The amphibole is Al poor ( $0.167–0.836$ ) and Mg rich ( $0.71 < X_{\text{Mg}} < 0.77$ ) and corresponds to Mg-hornblende and actinolite. The plagioclase is strongly zoned ( $6 < X_{\text{an}} < 59$ ).

##### 4.5. Mineral stability fields

Following the subdivisions proposed by Nachit et al. (1985), the analyzed biotites (Fig. 5) from the amphibole-biotite granitoid, the MME and the quartz jotunite dyke fall in the alkali-calcic (= subalkaline in French use) domain or on the boundary between this field and the calc-alkaline domain. The biotite granitoid is located on this boundary (sample F1) but also within the Al–K field (leucocratic variety, sample An 4).

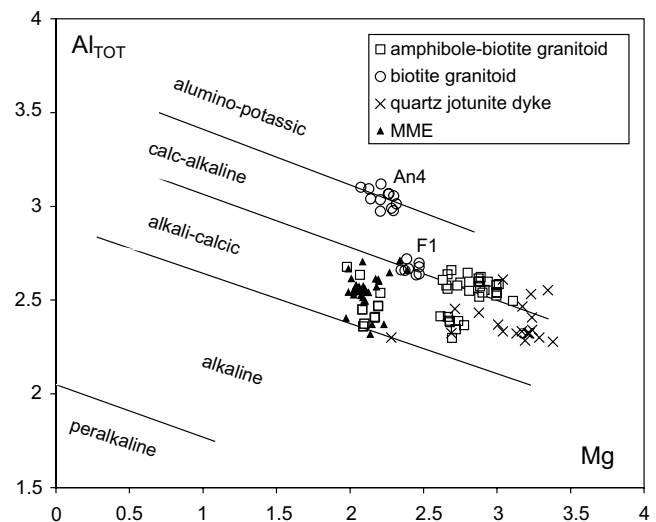


Fig. 5. Al–Mg diagram (atoms per formula unit) of biotites from the various Anfeq facies rocks. Fields from Nachit et al. (1985). An4 and F1 are sample names. MME = mafic microgranular enclave.

The Al-in hornblende barometer (calibrations of Hollister et al., 1987, and Schmidt, 1992) gives a pressure of about 4 kbar in granites and in MME. A value of  $7 \pm 1$  kbar is obtained in the amphibolite xenolith. The two thermobarometers based on Ti and Al<sup>VI</sup> in biotite (Schreus, 1985) and on Al exchange between plagioclase and amphibole (Holland and Blundy, 1994) give temperatures around 750 °C in nearly all plutonic facies. The destabilized biotite from the leucocratic biotite granite gives lower values between 750 and 650 °C. Amphibole bordering the orthopyroxene from the dyke gives temperatures between 700 and 650 °C, representing the opx destabilization. Amphibole from the amphibolite xenolith gives variable but higher temperatures between 750 and 890 °C.

## 5. Geochemistry

### 5.1. Analytical techniques

Sixteen samples have been analyzed for major and trace elements at CRPG, Nancy, France by ICP-AES and ICP-MS following Govindaraju and Mevelle (1987). Four samples (OT 47, OT 244, OT 14 and OT 19) were added from Cheilletz et al. (1992). The data are listed in Table 1. Following the IUGS recommendations, major elements have been recalculated to 100% without the loss of ignition (LOI) before use in the geochemical study.

Sr- and Nd-isotope analyses were carried out in the Isotope Geology laboratory from the Africa Museum, Tervuren. The samples were dissolved into a suboiled HF-HNO<sub>3</sub> acid mixture; if a solid phase remained after centrifugation, it was again dissolved into the same acid mixture but into teflon-lined stainless-steel digestion vessels at 180 °C. Sr and Nd were separated on SPEC<sup>®</sup> ion-exchange resins following a procedure adapted from Pin et al. (1994). Sr isotopic compositions were measured on single Ta filament and Nd isotopic compositions on triple Ta–Re–Ta filament using a Micromass Sector 54 multi-collector mass spectrometer. Repeated measurements of Sr and Nd standards showed that between-run error is better than  $\pm 0.000015$ . On each turret, four standards are measured together with 16 samples. The means of the four standards were used to correct the bias relatively to the recommended values (0.710250 for NBS987 and 0.511963 for the Rennes standard, corresponding to a La Jolla standard value of 0.511858). During this study, the NBS987 standard yielded values for <sup>87</sup>Sr/<sup>86</sup>Sr (normalized to <sup>86</sup>Sr/<sup>88</sup>Sr = 0.1194) from  $0.710261 \pm 0.000006$  to  $0.710287 \pm 0.000007$  ( $2\sigma$  on the mean; mean of  $0.710272 \pm 5$  on 16 standards), and the Rennes Nd standard <sup>143</sup>Nd/<sup>144</sup>Nd values (normalized to <sup>146</sup>Nd/<sup>144</sup>Nd = 0.7219) varied from  $0.511955 \pm 0.000007$  to  $0.511978 \pm 0.000006$  ( $2\sigma$  on

the mean; mean of  $0.511968 \pm 6$  on 17 standards). Rb and Sr concentrations were measured by X-ray fluorescence. The error on the Rb/Sr and Sm/Nd ratios is <4%. The Rb–Sr and Sm–Nd ages were calculated following Ludwig (1999). Used decay constants are  $1.42 \times 10^{-11} \text{ a}^{-1}$  (<sup>87</sup>Rb) and  $6.54 \times 10^{-12} \text{ a}^{-1}$  (<sup>147</sup>Sm). Sr and Nd isotope ratios are listed in Table 2.

### 5.2. Major and trace elements geochemistry

All the studied Anfege samples can be considered as mainly representing liquids: the MME have a doleritic texture, the quartz monzonite is fine-grained and appears as a dyke and the granitoids are quite differentiated and zones very rich in large feldspars have been avoided during sampling. Within the chemical diagram approaching the modal classification (Fig. 6A; Streckeisen and Le Maitre, 1979), the amphibole-biotite and biotite-granitoids extend from granodiorite to monzogranite. The MME are quartz monzodiorite as the dyke a quartz jotunite. The amphibolite xenolith is off the Anfege range, within the tonalitic field. The Anfege batholith as a whole lies close to the boundary between the subalkaline and the alkaline series of Kuno (1966) and below that of Irvine and Baragar (1971) (Fig. 6B). The sample B5 is low, which is a consequence of a low Na<sub>2</sub>O content (3.5%) for its silica content. The chemical classification proposed by Middlemost (1994) (Fig. 6B) is roughly compatible with that of Streckeisen and Le Maitre (1979) (Fig. 6A). The MME are rich in alkalis, richer than the extrapolated concentration at similar silica content of the granitoid trend where the quartz jotunite dyke is located (Fig. 6C). By contrast, the amphibolite xenolith is poorer in alkalis. The Anfege batholith displays a steep slope within the high-K calc-alkaline (HKCA) field (Fig. 6C). In addition to the MME (particularly D4) and the quartz monzonite, two biotite granitoids (An15 and OT19) lie above the main Anfege trend. The strong enrichment in K<sub>2</sub>O with silica suggests that K-feldspar was not at the liquidus. This is confirmed by Ba content: it shows a continuous and sharp increase with decreasing MgO (Fig. 6D). B5 amphibole-biotite granite seems to be abnormally rich in Ba but it is located within the main trend for K<sub>2</sub>O (Fig. 6C). This suggests rather that MgO content is too high in this sample, which is confirmed by the diagram opposing MgO to Fe<sub>2</sub>O<sub>3t</sub> (Fig. 6E). In the latter diagram, with the exception of this sample, one single trend is indeed observed for Anfege batholith. Here also the amphibolite xenolith lies well off the Anfege trend. Alumina (Fig. 6F) and CaO (not shown), decreases with MgO, indicating a plagioclase fractionation. B5 is here also far from the main trend. Zr and P<sub>2</sub>O<sub>5</sub> are positively correlated (Fig. 6G); the MME have the highest concentrations and are negatively correlated with SiO<sub>2</sub> (Table 1), suggesting a zircon-apatite fractionation. The

Table 1

Whole-rock geochemistry (major and trace elements) for the Anfég batholith; Xenolith = xenolith; MME = mafic microgranular enclave; Jot. = quartz jotunitite dyke

	Xeno.	MME			Jot.	Amphibole-biotite granitoid						Biotite granitoid								
	An11	D2	An10	D4	An7	B5	F4	B7	D5	An13	An6	OT14	OT47	OT19	AnF1	An15	C3	OT244	E1	A1
SiO <sub>2</sub>	62.53	55.74	59.92	59.63	59.51	64.37	69.13	69.56	69.85	70.62	70.87	71.91	65.41	66.84	67.02	68.42	69.31	69.56	70.90	70.78
TiO <sub>2</sub>	0.48	1.18	1.03	1.04	0.75	0.85	0.54	0.49	0.35	0.33	0.28	0.22	0.83	0.77	0.71	0.37	0.45	0.48	0.40	0.45
Al <sub>2</sub> O <sub>3</sub>	15.79	17.67	17.13	16.76	14.95	13.90	15.05	14.75	14.65	15.57	14.91	14.64	16.05	15.30	15.47	15.57	14.77	14.78	15.68	14.27
Fe <sub>2</sub> O <sub>3</sub>	2.06	2.66	2.51	2.42	2.32	2.19	1.09	1.08	1.02	0.98	0.98	0.80	1.79	1.52	1.56	1.17	1.13	1.11	0.81	1.11
FeO	4.31	4.32	4.02	3.62	4.04	3.78	1.38	1.33	1.31	1.30	1.19	0.86	2.64	1.93	2.14	1.44	1.46	1.45	1.04	1.26
MnO	0.11	0.15	0.11	0.14	0.10	0.15	0.06	0.04	0.04	0.04	0.03	0.03	0.08	0.07	0.07	0.03	0.06	0.05	0.02	0.05
MgO	2.83	2.72	2.34	2.36	5.66	3.47	0.75	0.92	0.86	0.68	0.82	0.28	1.77	1.45	1.47	0.91	0.94	0.91	0.65	0.84
CaO	5.80	5.32	4.84	4.18	5.53	3.89	2.22	2.11	2.46	2.30	1.47	1.36	3.76	3.15	2.85	2.51	2.22	2.48	2.40	0.72
Na <sub>2</sub> O	2.65	4.41	4.24	3.41	2.77	3.14	3.94	3.83	3.30	3.89	3.26	3.43	4.09	3.82	4.15	3.24	3.50	3.52	3.59	3.81
K <sub>2</sub> O	1.19	1.98	2.00	3.46	2.77	2.19	3.87	4.22	4.32	3.43	4.79	5.69	2.56	4.10	3.01	4.85	4.14	3.99	3.95	4.88
P <sub>2</sub> O <sub>5</sub>	0.20	0.38	0.30	0.24	0.29	0.21	0.18	0.21	0.12	0.19	0.19	0.08	0.34	0.26	0.28	0.15	0.16	0.11	0.11	0.21
LOI	1.52	1.56	1.06	1.24	0.81	0.64	0.98	0.82	1.18	0.97	1.02	0.40	0.51	0.54	0.44	1.12	0.98	1.06	0.59	1.05
Total	99.47	98.09	99.50	98.50	99.50	98.78	99.19	99.36	99.46	100.30	99.81	99.70	99.83	99.75	99.17	99.78	99.12	99.50	100.14	99.43
V	150	86	77	85	104	114	46	40	30	30	20				57	27	51		48	36
Rb	55	148	175	293	97	153	142	142	194	115	245	179	100	136	100	192	155	135	136	167
Y	16.0	50.8	29.3	45.0	15.0	29.0	6.0	11.7	13.7	9.4	12.0	5.1	23.3	24.6	13.6	10.9	31.0		5.0	19.8
Zr	78	308	266	219	182	219	204	207	147	179	140				261	159	177		221	227
Nb	2.2	34.2	19.6	25.8	7.7	18.9	9.0	12.9	9.9	6.3	10.3				12.6	8.3	21.0		5.0	15.8
Ba	330	321	323	543	788	816	807	1000	658	1054	693	1460	470	877	719	1009	747	1002	1515	1117
Co	16.7	15.1	16.0	19.0	23.9	20.0	6.0	5.4	4.7	2.6	4.0				9.3	5.1	7.0		2.0	5.0
Cr	23	37	8	41	476	262	64	59	56	6	35				101	19	70		110	73
Cu	42	22	69	35	27	3	4	16	6	5	14				14	5	7		5	10
Ga	16	34	29	27	20	24	23	25	23	25	24				24	22	22		22	20
Ni	12	7	9	9	79	32	4	10	5	4	9				10	7	10		4	8
Sn	1	13	10		2			5	4	2	18	1			2	4		2		2
W	0.39	0.46	0.14		0.44			0.59	0.38	0.11	4.16	0.20			0.71	0.42		0.10		0.65
Zn	51	148	132	135	75	144	50	53	50	63	53				72	54	56		33	50
La	7.9	60.5	51.2		40.4			71.0	30.8	46.1	42.1	37.8	63.1	41.9	69.1	37.0				52.6
Ce	17.8	124.6	100.3		77.7			122.1	56.2	90.6	70.0	66.8	113.8	82.3	137.6	66.1				93.5
Pr	2.3	15.2	11.4		8.4			13.0	5.9	9.7	8.4				14.9	6.8				10.4
Nd	10.2	61.1	43.3		30.9			46.2	23.7	34.6	27.3	26.1	53.7	42.8	55.0	23.8				38.0
Sm	2.42	13.18	7.68		5.14			7.53	4.53	5.65	5.09	4.00	9.70	7.60	8.56	3.91				7.43
Eu	0.70	2.15	1.84		1.33			1.38	0.99	1.34	0.90	1.00	2.10	1.70	1.51	1.15				1.50
Gd	2.34	10.86	5.57		3.79			4.92	3.22	3.14	3.26	2.90	7.10	6.10	5.96	2.46				5.11
Tb	0.32	1.59	0.85		0.56			0.64	0.45	0.43	0.44				0.74	0.37				0.73
Dy	2.24	8.99	4.63		2.91			2.80	2.45	2.06	2.13	1.20	4.30	4.00	3.47	1.72				3.78
Ho	0.48	1.97	0.88		0.53			0.47	0.51	0.31	0.36				0.52	0.35				0.74
Er	1.42	4.88	2.25		1.44			1.22	1.51	0.87	1.00	0.70	1.90	2.00	1.29	0.94				1.70
Tm	0.21	0.70	0.37		0.24			0.16	0.21	0.12	0.11				0.15	0.13				0.29
Yb	1.46	4.72	2.49		1.52			0.90	1.46	0.78	0.99	0.40	1.80	1.90	0.87	1.10				1.93
Lu	0.23	0.76	0.33		0.22			0.15	0.24	0.10	0.14	0.10	0.30	0.30	0.12	0.17				4.25
Hf	2.00	9.55	6.42		4.44			6.42	5.21	4.23	3.56				6.79	4.27				6.21
Ta	0.15	4.74	1.60		0.64			0.81	1.31	0.53	1.45				0.45	0.88				2.24
Pb	6.2	27.8	19.3	41.0	18.0	9.0	17.0	25.8	38.9	18.2	26.4				15.6	25.9	21.0		24.0	20.0
Th	1.7	16.8	14.2	10.0	12.8	15.0	7.0	23.4	20.9	10.3	21.6				11.7	16.4	17.0		15.0	13.6
U	0.41	4.57	3.26		1.64			2.94	4.64	1.02	5.74				2.53	2.19				3.03
Sr	312	231	268	188	367	364	422	444	273	711	225	271	594	512	416	330	379	623	788	338

The four samples "OT" are from Cheilletz et al. (1992).

Table 2  
Sr and Nd isotopic ratios for the Anfeg batholith

		Rb	Sr	<sup>87</sup> Rb/ <sup>86</sup> Sr	<sup>87</sup> Sr/ <sup>86</sup> Sr	±2σ	Sr <sub>i</sub> 608 Ma			
am-bi gr	B7	147	444	0.959	0.715162	0.000010	0.706848			
am-bi gr	D5	194	273	2.061	0.729131	0.000012	0.711262			
am-bi gr	An6	245	225	3.161	0.739126	0.000012	0.711719			
am-bi gr	An13	115	711	0.468	0.711877	0.000009	0.707817			
Q-jotun.	An7	97	367	0.765	0.715491	0.000009	0.708854			
bi gr	An15	192	330	1.686	0.724078	0.000012	0.709455			
bi gr	F1	100	416	0.696	0.712908	0.000010	0.706873			
bi gr	A1	167	338	1.432	0.720734	0.000009	0.708320			
MME	D2	148	231	1.857	0.724236	0.000009	0.708133			
xenolith	An11	55	312	0.510	0.709908	0.000010	0.705484			
		Sm	Nd	<sup>147</sup> Sm/ <sup>144</sup> Nd	<sup>143</sup> Nd/ <sup>144</sup> Nd	±2σ	ε <sub>Nd</sub> (608 Ma)	T <sub>CHUR</sub>	T <sub>DM</sub>	
am-bi gr	B7	7.53	46.16	0.0986	0.511996	0.000009	-4.91	998	1385	
am-bi gr	D5	4.53	23.66	0.1158	0.511707	0.000010	-11.89	1749	2080	
am-bi gr	An6	5.09	27.26	0.1129	0.511772	0.000011	-10.40	1572	1920	
am-bi gr	An13	5.65	34.65	0.0986	0.511794	0.000009	-8.85	1310	1651	
Q-jotun.	An7	5.14	30.89	0.1006	0.511796	0.000013	-8.97	1334	1678	
bi gr	An15	3.91	23.82	0.0993	0.511712	0.000009	-10.51	1446	1770	
bi gr	F1	8.56	55.01	0.0941	0.512081	0.000013	-2.89	827	1225	
bi gr	A1	7.43	37.95	0.1184	0.512082	0.000007	-4.76	1081	1532	
MME	D2	13.18	61.13	0.1304	0.511771	0.000007	-11.79	1987	2335	
xenolith	An11	2.42	10.21	0.1434	0.512586	0.000009	3.14	149	995	

T<sub>DM</sub> calculated following Nelson and DePaolo (1985).

amphibolite xenolith and the quartz jotunite dykes have higher P<sub>2</sub>O<sub>5</sub>/Zr ratios. The E1 sample is abnormally low in P<sub>2</sub>O<sub>5</sub> or rich in Zr. The sample B5 lies within the main trend, suggesting that its chemical peculiarities are due to feldspar proportion indicating a non-representativity of the analyzed powder. The samples B5 and E1 will not be studied further.

The amphibole-biotite and biotite granitoids share similar REE spectra (Fig. 7A and B) even if the former is slightly less rich than the latter (∑ REE = 181 and 222 ppm, respectively). Both are moderately to highly fractionated (La<sub>N</sub>/Yb<sub>N</sub>: 14–53 for amphibole-biotite granitoids, 15–54 for biotite granitoids), have no or slight Eu anomaly (Eu/Eu\* from 0.89 to 0.63 and 1.06 to 0.61, respectively), rather flat HREE (Ho<sub>N</sub>/Lu<sub>N</sub> from 0.94 to 1.40 + sample AnF1 at 1.96) and the HREE abundance is very low for the most differentiated samples (Lu<sub>N</sub> down to 2.6 and 3.1, respectively). All these characteristics are reminiscent of Archaean tonalites (Martin, 1987); as the Anfeg batholith is a Pan-African high-K calc-alkaline granitoid, this suggests that they correspond to the signature of the source. These REE spectra can be also correlated to the absence of K-feldspar at the liquidus (weak Eu anomaly) and to zircon fractionation (low HREE). Low HREE can be due also to a garnet-rich source.

The two analyzed MME have different REE patterns (Fig. 7C). Sample D2 (57% SiO<sub>2</sub>, poor in quartz xenocrysts), when compared to An10 (60.9% SiO<sub>2</sub>, rich in quartz xenocrysts), is richer in REE (∑ REE = 296 vs. 222 ppm), is less fractionated (La<sub>N</sub>/Yb<sub>N</sub> = 8.6 vs. 13.7)

and has a much larger negative Eu anomaly (Eu/Eu\* = 0.55 vs. 0.87). The sample An10, which appears more hybridised in the field, is richer in silica and displays a REE spectrum closer to that of granitoids. The chemical characteristics of the sample An10 are then likely to be the result of a mixing-mingling process, the sample D2 being a more pristine mafic magma. The latter has been selected for isotopic ratios measurement.

The quartz monzonitic dyke has a lower content in REE than the MME An10 (∑ REE = 167 vs. 222 ppm) but displays a similar REE pattern (Fig. 7C).

The amphibolite xenolith displays rather low REE content (∑ REE = 48 ppm), and a REE spectrum (Fig. 7D) slightly fractionated (La<sub>N</sub>/Yb<sub>N</sub> = 3.6), with a slight negative Eu anomaly (Eu/Eu\* = 0.91). This xenolith has lower contents in Y and Yb than MORB, only a slight increase from Yb to Ce, a Nb–Ta trough and a moderate enrichment in LILE, all features characteristic of island arc calc-alkaline basalts (Fig. 8A). It mimics indeed the composition of the Bogoslov Island (Aleutians arc) and of the Marianas arc basalts for elements from Th to Yb and is close for Sr, K, Rb and Ba. The latter elements have been probably mobile during the migmatization that affected this sample, explaining the less good fit.

The MME (Fig. 8B) do not have the same characteristics: Yb values are close to MORB values, a strong increase exists toward Ce (from 1 to 10), there is no Nb–Ta negative anomaly and they are richer in LILE although having lower SiO<sub>2</sub> content than the xenolith.

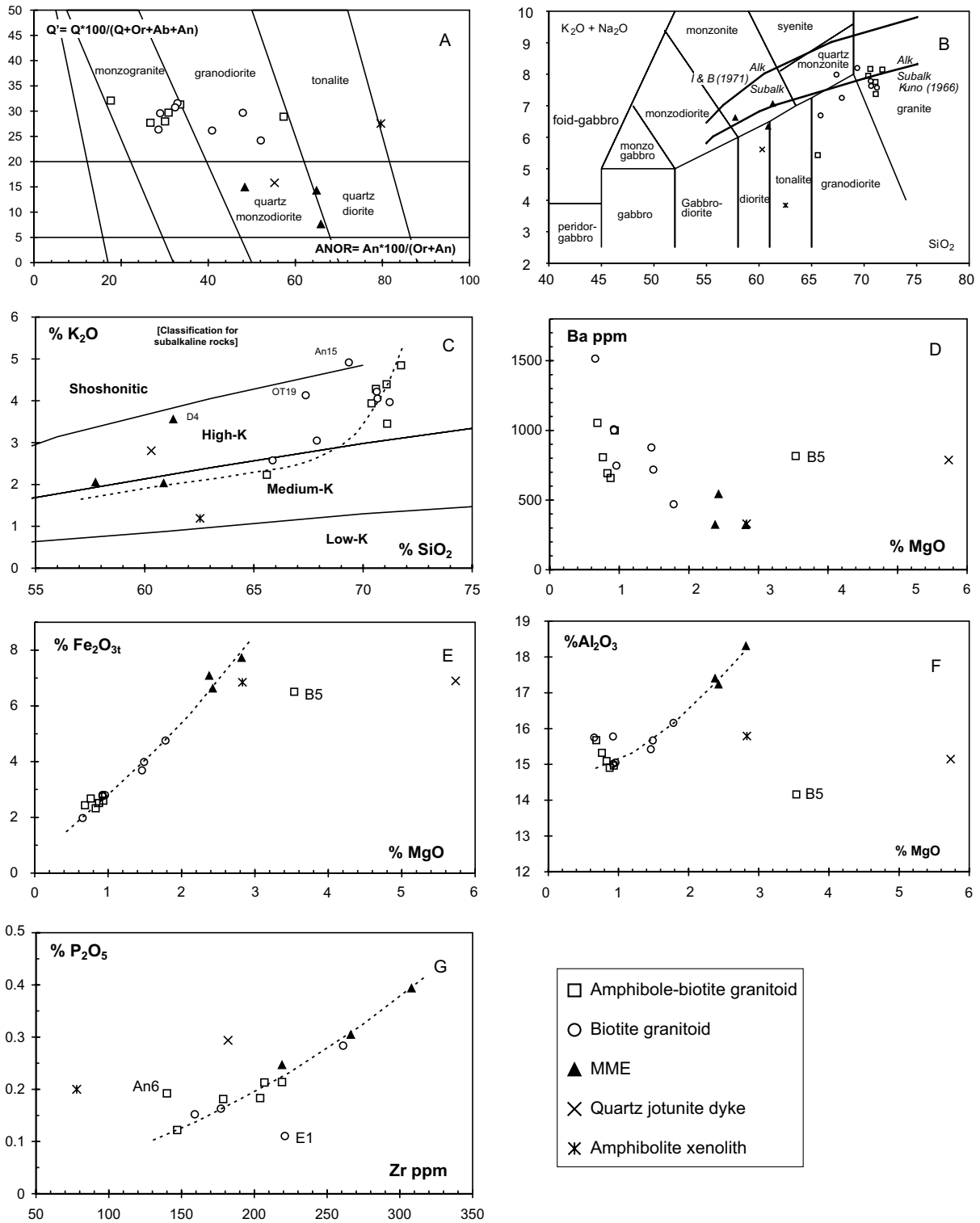


Fig. 6. XY diagrams allowing the chemical characterization of the Anfeg batholith. (A)  $Q'$ -Anor diagram (values from CIPW norm) following Streckeisen and Le Maitre (1979); (B)  $SiO_2$  vs.  $Na_2O + K_2O$ : petrological subdivisions from Middlemost (1994); alkaline-subalkaline boundary lines from Kuno (1966) and Irvine and Baragar (I&B, 1971); (C)  $SiO_2$  vs.  $K_2O$  (subdivisions from Rickwood, 1989); (D)  $MgO$  vs.  $Ba$ ; (E)  $MgO$  vs.  $Fe_2O_3$ ; (F)  $MgO$  vs.  $Al_2O_3$ ; (G)  $Zr$  vs.  $P_2O_5$ . Letters and digits close to some symbols are sample names.

The quartz jotunitic dyke is similar to MME, except for the presence of a Nb–Ta negative anomaly and lower Y–

Yb abundance. The source of the MME is then more enriched than that of the amphibolite xenolith.

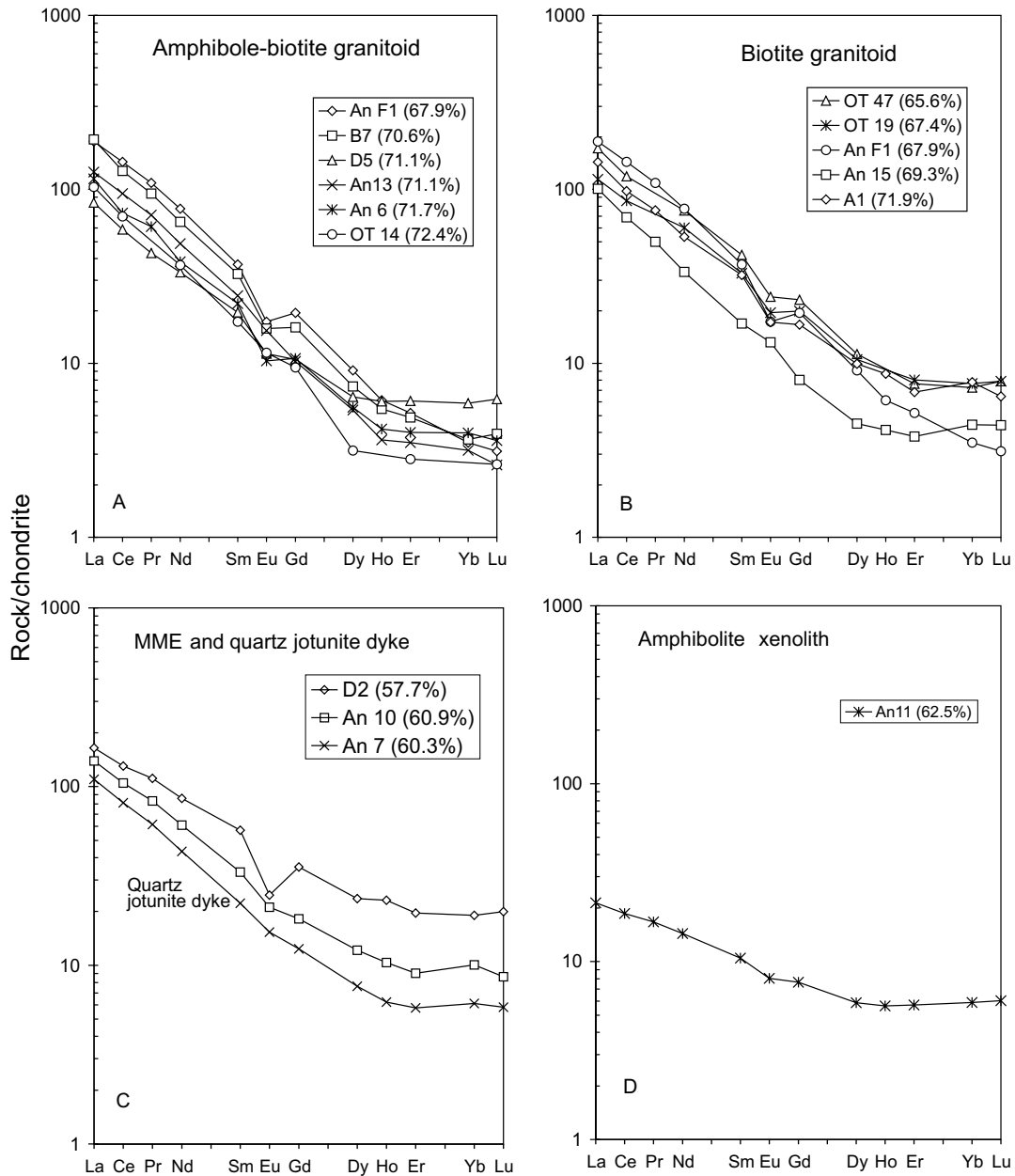


Fig. 7. Rare Earth normalized to chondrites diagrams: (A) amphibole-biotite granitoid; (B) biotite granitoid; (C) mafic magmatic enclaves (MME) and quartz jotunite dyke; (D) amphibolite xenolith. Percentage close to sample names are those of silica. OT samples are from Cheilletz et al. (1992). Normalizing values after Taylor and Mc Lennan (1985).

The amphibole-biotite and biotite granitoids have similar MORB-normalized spidergrams (Fig. 8C and D). Although at first sight close to MME patterns, some differences arise at a closer look: they are lower in Y and Yb, display Nb–Ta anomalies and are slightly less enriched in LREE.

Moreover, these granitoids have not the same silica contents, implying that these apparent similarities are actually differences. To overcome this bias, Liégeois et al. (1998) have proposed the use of the sliding normalization: each studied sample is normalized to an interpolated rock of a reference series having the same SiO<sub>2</sub>

content, to minimize the differentiation effect. This allows enhancing the differences existing between magmatic suites, taking into account the differentiation degree. They used as reference the alkali-calcic Yenchi-chi–Telabit series that we will adopt here too. For example, the Rb concentration of sample D5 (194 ppm for 69.85% SiO<sub>2</sub>) is divided by 140, which corresponds to the Rb concentration that would have a sample from the Yenchi-chi–Telabit series having 69.85% SiO<sub>2</sub> (calculated from the mean trend of the reference series through a second degree equation; see details in Liégeois et al., 1998).

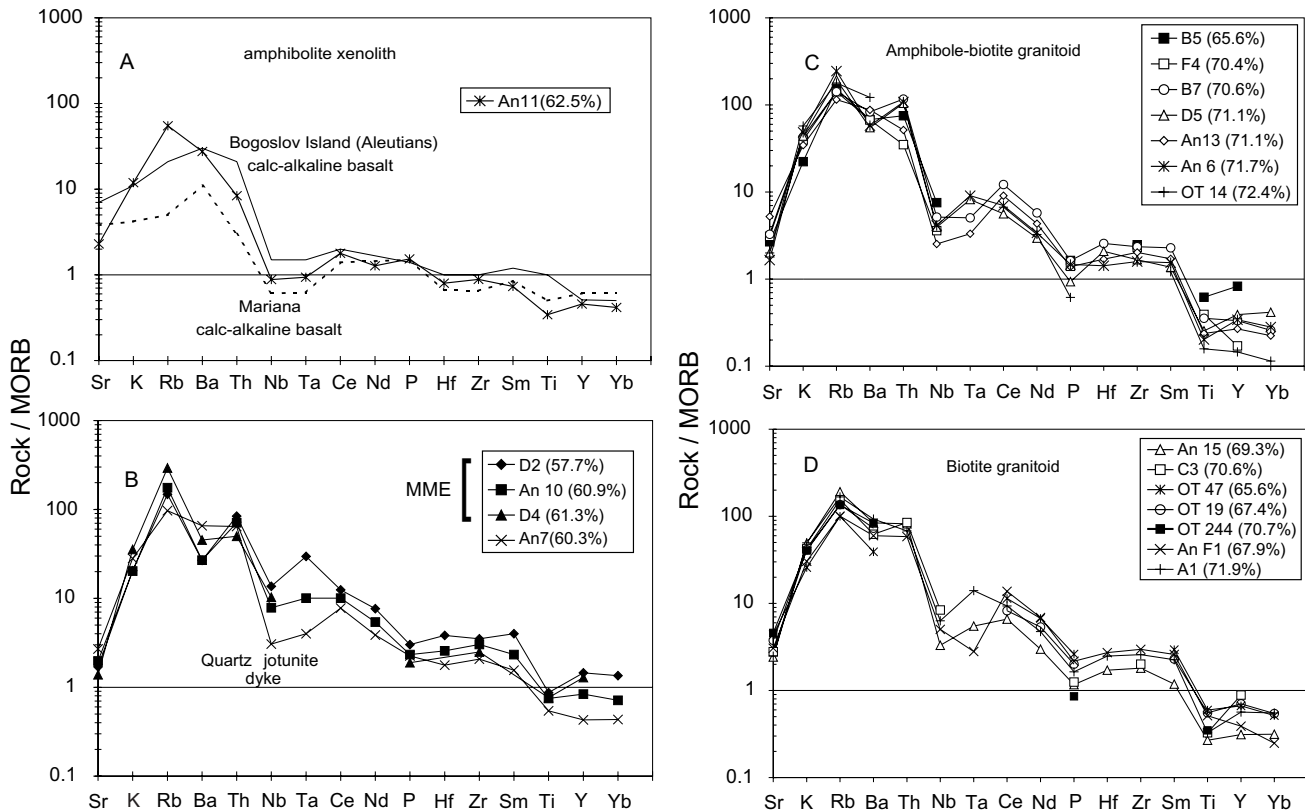


Fig. 8. Spidergram normalized to MORB (Sun and McDonough, 1989): (A) amphibolite xenolith; (B) mafic magmatic enclaves (MME) and quartz jotunite dyke; (C) amphibole-biotite granitoid; (D) biotite granitoid. OT samples are from Cheilletz et al. (1992). Bogoslov Island and Mariana basalts composition are from Pearce (1983).

In the synthetic *XY* diagram (Fig. 9A) grouping some selected NYTS (normalized to Yenchichi–Telabit series) elements, the Anfeq batholith determines a trend sub-parallel to the *Y* axis, which is typical for potassic (HKCA and shoshonitic) series and opposite to the trends developed by the alkaline–peralkaline series (Liégeois et al., 1998). The amphibolite xenolith is close to the origin, which agrees with its island arc signature (not potassic nor alkaline). In this diagram, the MME are strongly enriched when compared to the granitoids. They have values similar to the lower end of the Tertiary potassic basalts from Tibet (Turner et al., 1996). When detailing the situation by using spidergrams for the NYTS values (Fig. 9B–D), it appears that MME (Fig. 9B) have similar values than the reference series from Zr to Y and are enriched in Rb, Th, U, Ta, Nb, which is typical for potassic post-collisional series. This has been interpreted by Liégeois et al. (1998) as the result, during the post-collisional rise of isotherms, of the remelting of the lithospheric mantle previously enriched in K and associated elements by subduction or of lower crustal rocks derived from this modified lithospheric mantle. Turner et al. (1996) postulated a similar source for Tibet potassic basalts. The quartz jotunitic dyke does not show the same enrichments and the amphibolite xeno-

lith is low in all elements, particularly in Nb–Ta (Fig. 9B). The samples from the amphibole-biotite granitoid (Fig. 9C) display similar patterns from Nb to Y, being less enriched than the reference series (except An6 for Sm and Ce) with a strong depletion in Yb and Y. The latter depletion appears to be a characteristic of the Anfeq batholith. Concerning Rb, Th, U and Ta, the samples D5 and An6 are more enriched than the reference series while the sample An13 is low for all these elements and the sample B7 is intermediate. The sample An13 is particularly low in U, which could be linked to the greater mobility of this element in subsurface conditions. Similar observations can be made for the biotite granitoid (Fig. 9D). These results indicate that the Anfeq magmatic facies, even if some mobility of LILE can be suspected, belong to a low-HREE HKCA series. The quartz jotunitic dyke is similar to Anfeq granitoids while the amphibolite enclave is clearly xenolithic, as suspected in the field.

### 5.3. Nd and Sr isotopes

Sr and Nd isotopic ratios have been calculated back to 608 Ma, the U–Pb zircon age obtained on the Anfeq batholith (recalculated from Bertrand et al., 1986). In

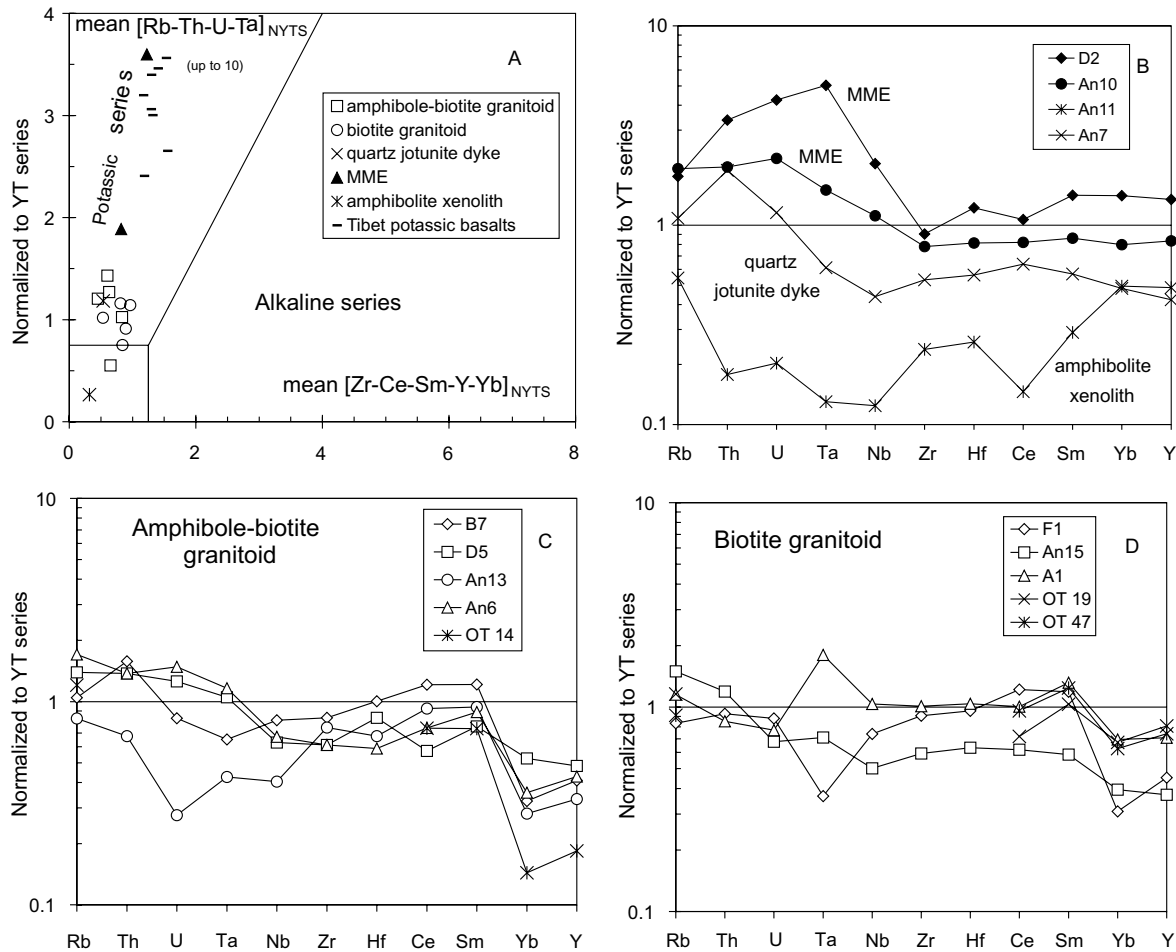


Fig. 9. Diagrams based on the sliding normalization (Liégeois et al., 1998): each element from the studied sample is normalized to the interpolated value from a reference series at the same silica content. The reference series used here is the Yenchichi–Telabit (YT) alkali-calcic series (see details in Liégeois et al., 1998). (A) Mean of NYTS (normalized to Yenchichi–Telabit series) values of Rb, U, Th, Ta vs. that of Zr, Ce, Sm, Y, Yb; limit between potassic and alkaline series from Liégeois et al. (1998); (B) Spidergram for NYTS values, mafic magmatic enclaves (MME) and quartz jotunitic dyke; (C) Spidergram for NYTS values, amphibole-biotite granitoid; (D) Spidergram for NYTS values, biotite granitoid. OT samples are from Cheilletz et al. (1992).

the  $\varepsilon_{\text{Nd}}$  vs.  $\text{Sr}_i$  diagram (Fig. 10A), the Anfeg batholith as a whole defines a continuous trend from  $-2.8/0.7068$  to  $-11.8/0.7111$ . The amphibole-biotite and biotite granitoids display samples all over the trend. The MME D2 (the poorest in quartz xenocrysts) is located at the low end ( $\varepsilon_{\text{Nd}} = -11.7$ ;  $\text{Sr}_i = 0.7079$ ). The quartz jotunitic dyke An7 lies on the same side ( $\varepsilon_{\text{Nd}} = -8.9$ ;  $\text{Sr}_i = 0.7088$ ). By contrast, the amphibolite xenolith An11 displays juvenile characteristics at 608 Ma ( $\varepsilon_{\text{Nd}} = +3.2$ ;  $\text{Sr}_i = 0.7054$ ).

## 6. Origin of the Anfeg batholith

The amphibolite enclave An11 is Neoproterozoic: its  $T_{\text{DM}} = 995$  Ma indicates the maximum age of intrusion, which will be younger if the mantle source of this sample is less depleted than DM (the most depleted mantle,  $\varepsilon_{\text{Nd}} = +7.8$  at 995 Ma). At 730 Ma, which is the age of

several island arc series in the Tuareg shield, the sample An11 has initial isotopic ratios close to oceanic island arc series ( $\varepsilon_{\text{Nd}} = +4.0$ ;  $\text{Sr}_i = 0.7046$ ), in agreement with its geochemical characteristics. This sample can thus be a xenolith from the Pan-African island arc series that were thrust onto the Laouni terrane at approximately 685 Ma (Liégeois et al., 2003, this issue).

In the  $\text{Sr}_i$  vs.  $\varepsilon_{\text{Nd}}$  diagram (Fig. 10A), the isotopic compositions at 608 Ma of three local references have been added: that from the Renatt potassic leucogranite (Aïr, Assodé-Issalane terrane, Fig. 1; Liégeois et al., 1994), from the Ounane granodiorite from northern LATEA (Gour Oumelalen area, Fig. 2; Liégeois et al., 2003, this issue) and from the Laouni ultramafic–mafic layered intrusions (southern Laouni terrane, Fig. 2; Cottin et al., 1998). In the Assodé-Issalane terrane, partial melts were generated within the granulitic lower crust; moving upward, they mixed and crystallized with autochthonous partial melts generated within the am-

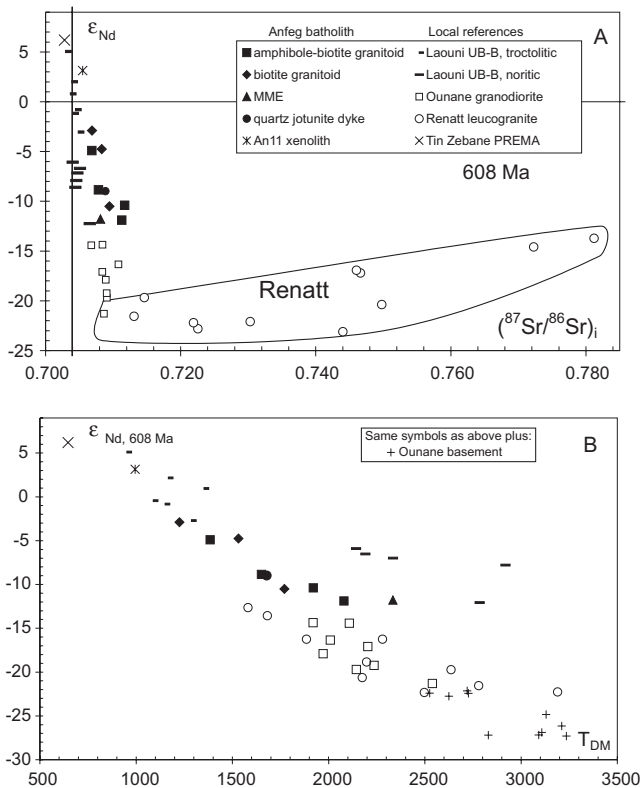


Fig. 10. Sr and Nd isotopic data for the different Anfeq facies granitoids and for local references. (A)  $\epsilon_{Nd}$  vs.  $(^{87}Sr/^{86}Sr)_i$ ; (B)  $\epsilon_{Nd}$  at 608 Ma vs.  $T_{DM}$  model ages. The isotopic ratios have been recalculated back to 608 Ma ago, the age of the Anfeq batholith emplacement. Reference values of Laouini from Cottin et al. (1998), Renatt from Liégeois et al. (1994), Tin Zebane from Hadj-Kaddour et al. (1998), Ounane from Liégeois et al. (2003, this issue) and Ounane basement from Peucat et al. (2003, this issue). PREMA = prevalent mantle.

phibolitic crust, giving birth to the Renatt potassic leucogranite (Rb–Sr isochron at approximately 666 Ma; Liégeois et al., 1994, 1998). This granite can then be considered as representing the lower and medium crusts within the Tuareg shield. At 608 Ma, this gives as mean for the lower crust:  $\epsilon_{Nd} = -23$ ;  $Sr_i = 0.710$  and for the medium crust:  $\epsilon_{Nd} = -15$ ;  $Sr_i = 0.780$ , all intermediates existing within the Renatt signature (Fig. 10A). The Ounane granodiorite intruded at approximately 624 Ma (Rb–Sr isochron, Liégeois et al., 2003, this issue) along a shear zone and its geochemical and Sr–Nd isotopic ratios ( $\epsilon_{Nd} = -17.3$ ;  $Sr_i = 0.7084$ ), indicate it resulted mainly from the melting of the LATEA Archaean–Palaeoproterozoic lower crust (Liégeois et al., 2003, this issue). The Laouini ultramafic–mafic layered complexes were emplaced into Anfeq-type granitoids in the south of the Laouini terrane (Fig. 2). Two magmatic liquid lines of descent are known (Cottin et al., 1998): a tholeiitic troctolitic trend (plagioclase–olivine–clinopyroxene cumulates) and a calc-alkaline noritic trend (orthopyroxene–plagioclase rich cumulates). The troctolitic series have mantle derived characteristics with only minor

lower crust contamination:  $Sr_i = 0.7030$  to  $0.7054$ ,  $\epsilon_{Nd} = +5$  to  $-1$ ; the noritic series shows stronger contamination by an Rb-depleted old crust:  $Sr_i = 0.7040$  to  $0.7065$ ,  $\epsilon_{Nd} = -7$  to  $-12$ .

The Anfeq batholith defines a trend parallel to the Laouini noritic series at slightly higher  $Sr_i$  for a given  $\epsilon_{Nd}$  (Fig. 10A). This trend spreads between the mainly mantle-derived Laouini troctolitic series and the Archaean–Palaeoproterozoic lower crust represented by the Ounane and Renatt granitoids. The Anfeq  $T_{DM}$  Nd model ages (Fig. 10B) range from 1225 Ma (biotite granitoid) to 2335 Ma (MME) joining again the Laouini troctolitic series ( $T_{DM} = 952$  to  $1353$  Ma; Cottin et al., 1998) and the Ounane granodiorite ( $T_{DM} = 1646$  to  $2322$  Ma; Liégeois et al., 2003) or the Renatt granite ( $T_{DM} =$  up to  $3189$  Ma; Liégeois et al., 1994). The extremity towards oldest  $T_{DM}$  of the two latter granitoids corresponds to the Archaean–Palaeoproterozoic granulitic gneisses from the Gour Oumelalen region (Red Gneiss Group), i.e. the Ounane country-rocks ( $T_{DM} = 2525$  to  $3236$  Ma; Peucat et al., 2003). If the quartz jotunite belongs to the Anfeq batholith, it could constitute the missing link between the Laouini layered complexes and the Anfeq batholith. Taking into account the above Tuareg reference reservoirs, the Sr–Nd isotopic compositions of the Anfeq batholith point to a mixing between melts generated within a juvenile mantle and an Archaean–Eburnian Rb-depleted granulitic lower crust.

The mantle source could correspond to that of the Laouini layered complexes (most depleted troctolitic sample:  $Sr_i = 0.7030$ ,  $\epsilon_{Nd} = +5.1$ ; Cottin et al., 1998). This mantle source is similar to that of approximately 592 Ma old Tin Zebane alkaline–peralkaline granitic dyke swarm (Hadj-Kaddour et al., 1998) and associated mafic rocks (Aït-Djafer et al., 2003) in western Hoggar that possesses a prevalent mantle (PREMA; Zindler and Hart, 1986) source isotopic composition ( $Sr_i = 0.7028$ ,  $\epsilon_{Nd} = +6.2$ ). The old Rb-depleted crustal source corresponds to the LATEA granulitic lower crust known in the Gour Oumelalen area and whose melting produced the low  $Sr_i$  Renatt end-member (at 608 Ma,  $Sr_i = 0.708$ ,  $\epsilon_{Nd} = -22$ ). The Archaean-like REE patterns of Anfeq (Fig. 7A and B) could be a signature of this old source. Paradoxically, the lower crust/mantle ratio was higher in the MME (sample D2:  $\epsilon_{Nd} = -11.8$ ,  $T_{DM} = 2335$  Ma) than in some biotite granitoids (sample F1:  $\epsilon_{Nd} = -2.9$ ,  $T_{DM} = 1225$  Ma).

## 7. Emplacement of the Anfeq batholith during the metacratonization of LATEA

### 7.1. LATEA metacratonization

Made of Archaean and Eburnian lithologies (Bertrand et al., 1986; Peucat et al., 2003, this issue), the

LATEA microcontinent behaved as a passive margin during the Pan-African orogeny (Liégeois et al., 2003, this issue). During the Neoproterozoic, LATEA has been submitted to several episodes of island arc accretions among which is the Tin Begane eclogite-bearing sheets thrust at approximately 685 Ma to the south of Anfeq (Fig. 2; Liégeois et al., 2003, this issue). Final squeezing of LATEA between the West African craton (WAC) to the west and the Saharan craton (SC) to the east led to a general escape of the Tuareg terranes to the north mainly in the 620–580 Ma period (Black et al., 1994; Liégeois et al., 1998). This period began just after the initial collisional impact with the WAC which is dated by the eclogites thrust on it at approximately 625 Ma (Jahn et al., 2001). This continental scale transpressive squeezing did not induce a major lithospheric or crustal thickening in LATEA, the “in situ” Pan-African metamorphism on the old basement being limited to greenschist facies, lower amphibolite facies, stronger Pan-African metamorphism being only found in allochthonous oceanic nappes (Liégeois et al., 2003, this issue).

The main approximately 600 Ma events are the sub-vertical mega-shear zones dissecting LATEA and the emplacement of the Anfeq- and Ounane-type granitoids. This corresponds to the notion of metacraton proposed by Abdelsalam et al. (2002), i.e. a craton partly destabilized and having lost partially its cratonic characteristics (rigidity, absence of major younger events, platform sediments, etc.) but being still recognisable.

### 7.2. Intrusion of the Anfeq batholith

The Anfeq batholith can then be considered as post-collisional, knowing that the collision itself had limited effects in the LATEA microcontinent. Characteristically, Anfeq ( $\approx 608$  Ma) intruded much older basement (1.9 Ga and older) mainly along subhorizontal structures and could be described as a large composite laccolith (Fig. 3). However, close to the subvertical shear zones, the foliation affecting Anfeq becomes also sub-vertical even if it is a largely subsolidus tectonic structure. These subvertical shear zones inside and bordering the Laouni terrane can be considered as the pathway for the magma before it spread horizontally along thrust planes. Although additional structural observations coupled with ASM measurements should be done to test the model in Hoggar, a strike-slip partitioned transpression (McCaffrey, 1996; Teyssier and Tikoff, 1998) could meet the above observations (Fig. 11): in a strike-slip transpression system, in the lower ductile crust the transpression is accommodated by distributed shear that can favour upward magma movement; in the upper brittle layer, the transpression is partitioned with the strike-slip component taken up on the vertical shear zone and shortening taken up on a thrust system oblique

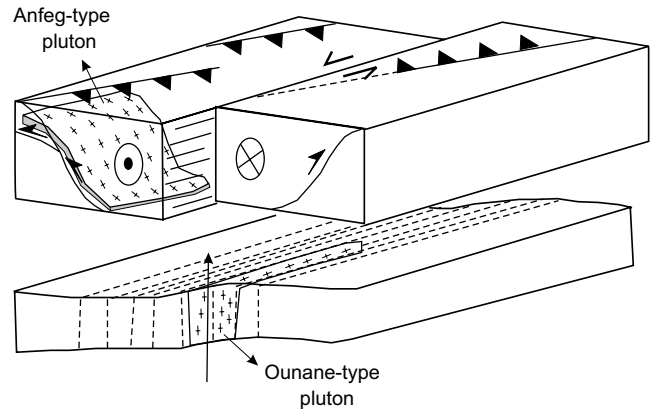


Fig. 11. Model for the emplacement of the Anfeq batholith within a thrust structure associated with a major strike-slip partitioned transpression (McCaffrey, 1996). Abundant magmatism would be able to cause vertical migration of the attachment zone (Garde et al., 2002) and to determine its localization (Anfeq case). When less abundant, the granitoid plutons are more often located within the subvertical shear zone (Ounane case).

to the fault, favouring lateral horizontal spreading of the magmas. At the base of this partitioned system is localized an attachment or coupling zone (Teyssier et al., 2002). The small Tifferkit pluton close to Anfeq (Fig. 3), as the larger Ounane in the Gour Oumelalen region (Fig. 2), is limited to the subvertical shear zone. This suggests that Anfeq intruded not far from the attachment. This is not surprising as the depth of the attachment is strongly depending on the geothermal gradient, itself largely affected by magma intrusions when abundant. Large granitic masses will then be able to cause vertical migration of this attachment zone (Garde et al., 2002). Such a link between granitoid batholiths and mega-shear zones is a characteristic of the post-collisional period (Liégeois, 1998 and references therein). This is particularly spectacular in the LATEA case as this cratonic microcontinent has been involved into such a post-collisional setting without having been transformed before into an active margin. LATEA could be compared with the Tarim basin to the north of Tibet, which is characterized by a thicker lithospheric mantle and a more rigid behaviour than the surrounding terranes (e.g. Molnar, 1988).

### 7.3. Melting of the Anfeq source

The large movements along the mega-shear zones affecting the whole lithosphere of LATEA metacraton can be the cause of the melting of the Anfeq source(s): it is known in the current major shear zones that they are characterized by high heat flow due to the presence of asthenosphere at shallow depth, not far from the Moho (e.g. Lachenbruch et al., 1985 for San Andreas fault; Leloup and Kienast, 1993 for the Ailo Shan—Red River

fault). This can be related to a linear lithospheric delamination along the shear zone, allowing the asthenosphere to rise (Black and Liégeois, 1993) up to the Moho if the major coupling zone is the crust–lithosphere boundary (Bird, 1979). In that case, the asthenosphere itself can melt by adiabatic pressure release and can melt the lower crust, either mafic or felsic, either old or young, due to the high heat flow generated. In the Anfeq case, both asthenospheric mantle and Archaean–Eburnian crust melted and mixed in variable amounts.

#### 7.4. Gradient of mantle and crust contribution in the Pan-African plutons in LATEA

In LATEA, there is a gradient from northeast to southwest (Fig. 2): to the northeast (Egéré-Aleksod terrane), the Pan-African granitoids are rare, limited to the shear zones and their source is mainly the LATEA Archaean–Eburnian lower crust (e.g. Ounane pluton; Liégeois et al., 2003, this issue); more to the southwest (Tefedest and Laouni terranes), the granitoids are more numerous and expanded laterally along subhorizontal thrust structures, being abundant enough to control the depth of the attachment zone. This is the case with Anfeq, which contains a greater amount of asthenospheric component in its parental magma (Fig. 10A); at the southern edge of LATEA, nearly uncontaminated asthenospheric melts were emplaced (Laouni troctolitic suites; Cottin et al., 1998). As shown by the Laouni layered complexes that contain also a noritic series quite strongly contaminated by the lower crust, this gradient is a mean; in each case, variable mantle/crust melt ratios can exist, showing that a common process was at work from north to south of LATEA.

What was located to the south of LATEA is not known as it is currently buried under the Phanerozoic Iullemeden sedimentary basin (Fig. 1). However the NE movement of the oceanic thrust sheets (Bertrand et al., 1986; Liégeois et al., 2003, this issue) and the presence of the Tessalit ophiolite close to the Laouni layered complexes to the south (Fig. 2) suggest that the southern boundary of LATEA was not located much further south. A more intense metacratonization in the south of LATEA than in the north is then likely.

## 8. Conclusion

The Anfeq granodioritic to granitic batholith is a syn-kinematic composite laccolith that intruded at approximately 4 kbar, 608 Ma ago (recalculated from Bertrand et al., 1986), along subhorizontal thrust planes associated with subvertical mega-shear zones. The latter were generated by the main transpressive phase that corresponds to the general escape of the Tuareg terranes to

the north (Black et al., 1994). Parts of Anfeq and some plutons (Tifferkit) are located within the subvertical shear zones. The abundance of such batholiths in the area allows suggesting that they have controlled the attachment depth of a strike-slip partitioned transpression (McCaffrey, 1996; Teyssier and Tikoff, 1998; Garde et al., 2002).

There is a strong contrast in age between Anfeq ( $\approx 608$  Ma) and its high-grade country-rocks (1.9 Ga or older), belonging to the LATEA microcontinent. Neoproterozoic lithologies are restricted to island arc sheets thrust upon the old LATEA basement, only locally affected by this accretion event (Liégeois et al., 2003, this issue). With the exception of these thrust sheets, the Pan-African orogeny in LATEA is of post-collisional nature (sensu Liégeois et al., 1998): large horizontal movements along subvertical shear zones, high temperature metamorphism, HKCA magmatism. In the LATEA case, these events have largely preserved the old basement where Eburnian fresh high-pressure granulitic parageneses can be found (Ouzegane et al., 2001). The Pan-African orogeny is then responsible for the dismembering of LATEA former passive margin (Liégeois et al., 2003, this issue), leading to its metacratonization (Abdelsalam et al., 2002).

The geochemical and Sr–Nd isotopic signature of the Anfeq batholith points to a mixed mantle–old crust origin whose end-members have been identified within LATEA and elsewhere in the Tuareg shield (asthenospheric PREMA mantle and Archaean–Palaeoproterozoic Rb-depleted granulitic crust from LATEA). The model proposed consists in a linear lithospheric delamination along the mega-shear zones dissecting LATEA microcontinent allowing the asthenosphere to rise close to Moho. This allows the melting of the LATEA lower crust due to the consequent high heat flow and of the asthenosphere itself by adiabatic pressure release. This model of metacratonization of a former passive margin can be extended to the whole LATEA microcontinent with stronger effects to the southwest (southern Laouni terrane) with nearly uncontaminated mantle melts (Cottin et al., 1998) than to the northeast (Northern Egéré-Aleksod terrane, Gour Oumelalen area) where granitoids are much less abundant and nearly entirely generated within the LATEA old lower crust (Liégeois et al., 2003, this issue).

The Anfeq case study indicates that HKCA batholiths can be produced in a non-active margin setting, i.e. in a former passive margin being metacratonized during a post-collisional period.

## Acknowledgements

We would like to thank J. Boissonnas for judicious comments and for help with the English. A. Cheilletz

and J. Dostal are acknowledged for their constructive reviews, which ameliorated this article. This work is a contribution to project “Héritage éburnéen et structuration panafricaine du Hoggar: étude géologique et géophysique” supported by the French-Algerian cooperation program 00MDU476. This is a contribution to IGCP485 and to NATO project EST/CLE 979766.

## References

- Abdelsalam, M., Liégeois, J.P., Stern, R.J., 2002. The Saharan metacraton. *Journal of African Earth Sciences* 34, 119–136.
- Aït-Djafer, S., Ouzegane, K., Liégeois, J.P., Kienast, J.R., 2003. An example of post-collisional mafic magmatism: the gabbro-anorthosite layered complex from the Tin Zebane area (western Hoggar, Algeria). *Journal of African Earth Sciences*, this issue.
- Azzouni-Sekkal, A., Boissonnas, J., 1993. Une province magmatique de transition du calco-alcalin à l'alcalin: les granitoïdes pan-africains à structure annulaire de la chaîne pharusienne du Hoggar (Algérie). *Bulletin Société Géologique France* 164, 597–608.
- Azzouni-Sekkal, A., Liégeois, J.P., Bechiri-Benmerzoug, F., Belaidi-Zinet, S., Bonin, B., 2003. The “Taourirt” magmatic province, a marker of the very end of the Pan-African orogeny in the Tuareg Shield: review of the available data and Sr–Nd isotope evidence. *Journal of African Earth Sciences*, this issue.
- Ba, H., Black, R., Benziane, B., Diombana, D., Hascoet-Fender, J., Bonin, B., Fabre, J., Liégeois, J.P., 1985. La province des complexes annulaires alcalins sursaturés de l'Adrar des Iforas, Mali. *Journal of African Earth Sciences* 3, 123–142.
- Belhai, D., Ouzegane, K., 2000. Structural analysis and metamorphic evolution in the Tin Begane granulite complex, Central Hoggar, Algeria. *Journal of African Earth Sciences* 30 (4), 11.
- Bertrand, J.M., Michard, A., Boullier, A.M., Dautel, D., 1986. Structure and U/Pb geochronology of Central Hoggar (Algeria): a reappraisal of its Pan-African evolution. *Tectonics* 5, 955–972.
- Bird, P., 1979. Continental delamination and the Colorado plateau. *Journal of Geophysical Research* 84, 7561–7571.
- Black, R., Liégeois, J.P., 1993. Cratons, mobile belts, alkaline rocks and continental lithospheric mantle: the Pan-African testimony. *Journal of the Geological Society of London* 150, 89–98.
- Black, R., Latouche, L., Liégeois, J.P., Caby, R., Bertrand, J.M., 1994. Pan-African displaced terranes in the Tuareg shield (central Sahara). *Geology* 22, 641–644.
- Caby, R., 1996. A review of the In Ouzal granulitic terrane (Tuareg shield, Algeria): its significance within the Pan-African Trans-Saharan belt. *Journal of Metamorphic Geology* 14, 659–666.
- Caby, R., Andreopoulos-Renaud, U., 1987. Le Hoggar oriental, bloc cratonisé à 730 Ma dans la chaîne pan-africaine du Nord du continent africain. *Precambrian Research* 36, 335–344.
- Caby, R., Andreopoulos-Renaud, U., Pin, C., 1989. Late Proterozoic arc-continent and continent–continent collision in the Pan-African Trans-Saharan belt of Mali. *Canadian Journal of Earth Sciences* 26, 1136–1146.
- Cheilletz, A., Bertrand, J.M., Charoy, B., Moulahoum, O., Bouabsa, L., Farrar, E., Zimmerman, J.L., Dautel, D., Archibald, D.A., Boullier, A.M., 1992. Géochimie et géochronologie Rb–Sr, K–Ar et <sup>39</sup>Ar–<sup>40</sup>Ar des complexes granitiques Pan-Africains de la région de Tamanrasset (Algérie): relations avec les minéralisations Sn–W associées et l'évolution tectonique du Hoggar central. *Bulletin Société Géologique France* 163, 733–750.
- Cottin, J.Y., Lorand, J.P., Agrinier, P., Bodinier, J.L., Liégeois, J.P., 1998. Isotopic (O, Sr, Nd) and trace element geochemistry of the Laouini layered intrusions (Pan-African belt, Hoggar, Algeria): evidence for post-collisional tholeiitic magmas variably contaminated by continental crust. *Lithos* 45, 197–222.
- Garde, A.A., Chadwick, B., Grocott, J., Hamilton, M.A., McCaffrey, K.J.W., Swager, C.P., 2002. Mid-crustal partitioning and attachment during oblique convergence in an arc system, Palaeoproterozoic Ketilidian orogen, southern Greenland. *Journal of the Geological Society of London* 159, 247–261.
- Govindaraju, K., Mevelle, G., 1987. Fully automated dissolution and separation methods for inductively coupled plasma atomic emission spectrometry rock analysis. Application to the determination of rare earth elements. *Journal of Analytical Atomic Spectrometry* 2, 615–621.
- Guérangé, B., Byramjee, R., 1957. Feuille au 1/200 000° Fort Laperrière. Mission Hélicoptère. Hoggar 1956–57, Rapport BRMA.
- Hadj-Kaddour, Z., Demaiffe, D., Liégeois, J.P., Caby, R., 1998. The alkaline–peralkaline granitic post-collisional Tin Zebane dyke swarm (Pan-African Tuareg shield, Algeria): prevalent mantle signature and late aegaitic differentiation. *Lithos* 45, 223–243.
- Holland, T., Blundy, J., 1994. Nonideal interactions in calcic amphiboles and their bearing on amphibole–plagioclase thermometry. *Contributions to Mineralogy and Petrology* 116, 433–447.
- Hollister, L.S., Grissom, G.C., Peters, E.K., Stowell, H.H., Sisson, V.B., 1987. Confirmation of the empirical correlation of Al-in hornblende with pressure of solidification of calc-alkaline plutons. *American Mineralogist* 72, 231–239.
- Irvine, T.N., Baragar, W.R.A., 1971. A guide to the chemical classification of the common volcanic rocks. *Canadian Journal of Earth Sciences* 8, 523–548.
- Jahn, B.M., Caby, R., Monié, P., 2001. The oldest UHP eclogites of the world: age of UHP metamorphism, nature of protoliths and tectonic implications. *Chemical Geology* 178, 143–158.
- Kienast, J.R., Fourcade, S., Guiraud, M., Hensen, B.J., Ouzegane, K., 1996. Journal of Metamorphic Geology 14, 144, Special issue on the In Ouzal granulite unit, Hoggar, Algeria.
- Kuno, H., 1966. Lateral variations of basalt magma type across continental margins and island arcs. *Bulletin Volcanologique* 29, 195–222.
- Lachenbruch, A.H., Sass, J.H., Galanis Jr., S.P., 1985. Heat flow in southernmost California and the origin of the Salton trough. *Journal of Geophysical Research* 90, 6709–6736.
- Latouche, L., Vidal, P., 1974. Géochronologie du Précambrien de la région des Gour Oumelalen (Nord-Est de l'Ahaggar, Algérie). Un exemple de mobilisation du strontium radiogénique. *Bulletin Société Géologique France* 16, 195–203.
- Leloup, P.H., Kienast, J.R., 1993. High temperature metamorphism in a major strike-slip shear zone: the Ailao Shan—Red River, People's Republic of China. *Earth and Planetary Science Letters* 118, 213–234.
- Liégeois, J.P., 1998. Some words on the post-collisional magmatism. *Lithos* 45, xv–xviii.
- Liégeois, J.P., Bertrand, J.M., Black, R., 1987. The subduction- and collision-related Pan-African composite batholith of the Adrar des Iforas (Mali). A review. *Geological Journal* 22, 185–211.
- Liégeois, J.P., Black, R., Navez, J., Latouche, L., 1994. Early and late Pan-African orogenies in the Air assembly of terranes (Tuareg shield, Niger). *Precambrian Research* 67, 59–88.
- Liégeois, J.P., Diombana, D., Black, R., 1996. The Tessalit ring complex (Adrar des Iforas, Malian Tuareg shield): a Pan-African, post-collisional, syn-shear, alkaline granite intrusion. In: Demaiffe, D. (Ed.), *Petrology and Geochemistry of Magmatic Suite of Rocks in the Continental and Oceanic Crusts*. ULB-MRAC, Bruxelles, pp. 227–244.
- Liégeois, J.P., Navez, J., Hertogen, J., Black, R., 1998. Contrasting origin of post-collisional high-K calc-alkaline and shoshonitic versus alkaline and peralkaline granitoids. *Lithos* 45, 1–28.
- Liégeois, J.P., Latouche, L., Boughrara, M., Navez, J., Guiraud, M., 2003. The LATEA metacraton (Central Hoggar, Tuareg shield,

- Algeria): behaviour of an old passive margin during the Pan-African orogeny. *Journal of African Earth Sciences*, this issue.
- Ludwig, K.R., 1999. Using Isoplot/Ex Version 2.01, A Geochronological Toolkit for Microsoft Excel. In: Special Publication 1a. Berkeley Geochronology Center. 47 p.
- Martin, H., 1987. Archaean and modern granitoids as indicators of changes in geodynamic processes. *Revista Brasileira Geociencias* 17, 360–365.
- McCaffrey, R., 1996. Slip partitioning at convergent plate boundaries of SE Asia. In: Hall, R., Blundell, D.J. (Eds.), *Tectonic Evolution of Southeast Asia*. In: Special Publication 106. Geological Society of London, pp. 3–18.
- Middlemost, E.A.K., 1994. Naming material in the magma/igneous rock system. *Earth-Science Review* 37, 215–224.
- Molnar, P., 1988. A review of geophysical constraints on the deep structure of the Tibetan plateau, the Himalaya and the Karakoram, and their tectonic implications. *Philosophical Transactions of the Royal Society of London, Series A* 326, 33–88.
- Moulahoum, O., 1988. Dualité du magmatisme d'âge panafricain: aspects structuraux et pétrologique des granites subalcalins et alumineux de la région de Tamanrasset (Hoggar central, Algérie). Thesis, Université Nancy I, France, 145 p.
- Nachit, H., Razafimahefa, N., Stussi, J.M., Caron, J.P., 1985. Composition chimique des biotites et typologie magmatique des granitoïdes. *Comptes Rendus Académie des Sciences Paris* 301, 813–818.
- Nelson, B.K., DePaolo, D.J., 1985. Rapid production of continental crust 1.7–1.9 b.y. ago: Nd isotopic evidence from the basement of the North American Midcontinent. *Geological Society of America Bulletin* 96, 746–754.
- Ouzegane, K., Boumaza, S., 1996. An example of ultrahigh-temperature metamorphism: orthopyroxene–sillimanite–garnet, sapphirine–quartz parageneses in Al–Mg granulites from In Hihaou, In Ouzal, Hoggar. *Journal of Metamorphic Geology* 14, 693–708.
- Ouzegane, K., Bendaoud, A., Kienast, J.R., Touret, J.L.R., 2001. Pressure–temperature–fluid evolution in the Eburnean metabasites and metapelites from Tamanrasset (Hoggar, Algeria). *Journal of Geology* 109, 247–263.
- Paquette, J.L., Caby, R., Djouadi, M.T., Bouchez, J.L., 1998. U–Pb dating of the end of the Pan-African orogeny in the Tuareg shield: the post-collisional syn-shear Tiouéine pluton (Western Hoggar, Algeria). *Lithos* 45, 245–254.
- Pearce, J., 1983. Role of the sub-continental lithosphere in magma genesis at active continental margins. In: Hawkesworth, C.J., Norry, M.J. (Eds.), *Continental Basalts and Mantle Xenoliths*, Shiva Geology Series. Nantwich, pp. 230–249.
- Peucat, J.J., Drareni, A., Latouche, L., Deloué, E., Vidal, P., 2003. U–Pb zircon (TIMS and SIMS) and Sm–Nd whole-rock geochronology of the Gour Oumelalen granulitic basement, Hoggar massif, Tuareg shield, Algeria. *Journal of African Earth Sciences*, this issue.
- Pin, C., Briot, D., Bassin, C., Poitrasson, F., 1994. Concomitant separation of strontium and samarium–neodymium for isotopic analysis in silicate samples, based on a specific extraction chromatography. *Analytica Chimica Acta* 298, 209–217.
- Rickwood, P.C., 1989. Boundary lines within petrologic diagrams which use oxides of major and minor elements. *Lithos* 22, 247–264.
- Schmidt, M.W., 1992. Amphibole composition in tonalite as a function of pressure: an experimental calibration of Al-in hornblende barometer. *Contributions to Mineralogy and Petrology* 110, 304–310.
- Schreus, J., 1985. Prograde metamorphism of metapelites, garnet–biotite thermometry and prograde changes of biotite chemistry in high-grade rocks of West Uusimaa, southwest Finland. *Lithos* 18, 69–80.
- Streckeisen, A., Le Maitre, R.W., 1979. A chemical approximation to the modal QAPF classification of the igneous rocks. *Neues Jahrbuch Mineralogie Abhandlungen* 136, 169–206.
- Sun, S.S., McDonough, W.F., 1989. Chemical and isotopic systematics of oceanic basalts: implication for mantle composition and processes. In: Saunders, A.D., Norry, M.J. (Eds.), *Magmatism in Ocean Basins*. In: Special Publication 42. Geological Society London, pp. 313–345.
- Taylor, S.R., Mc Lennan, S.M., 1985. *The Continental Crust: Its Composition and Evolution*. Blackwell, Oxford. 312 p.
- Teyssier, C., Tikoff, B., 1998. Strike-slip partitioned transpression of the San Andreas fault system: a lithospheric approach. In: Holdsworth, R.E., Strachan, R.A., Dewey, J.F. (Eds.), *Continental Transpressional and Transtensional Tectonics*. In: Special Publication 135. Geological Society of London, pp. 143–158.
- Teyssier, C., Tikoff, B., Weber, J., 2002. Attachment between brittle and ductile crust at wrenching plate boundaries. In: Bertotti, G., Schulman, K., Cloething, S. (Eds.), *Continental Collision and the Tectono–Sedimentary Evolution of Forelands*. In: Special Publications 1. European Geophysical Society, pp. 93–117.
- Turner, S., Arnaud, N., Liu, J., Rogers, N., Hawkesworth, C., Harris, N., Kelley, S., Van Calsteren, P., Deng, W., 1996. Post-collision, shoshonitic volcanism on the Tibetan plateau: implications for convective thinning of the lithosphere and the source of ocean island basalts. *Journal of Petrology* 37, 45–71.
- Zindler, A., Hart, S.R., 1986. Chemical geodynamics. *Annual Review of Earth and Planetary Sciences* 14, 493–571.